

1 Source attribution of near-surface ozone trends in the
2 United States during 1995–2019

3
4
5
6 Pengwei Li¹, Yang Yang^{1*}, Hailong Wang², Su Li¹, Ke Li¹, Pinya Wang¹, Baojie
7 Li¹, Hong Liao¹

8
9
10 ¹Jiangsu Key Laboratory of Atmospheric Environment Monitoring and
11 Pollution Control, Jiangsu Collaborative Innovation Center of Atmospheric
12 Environment and Equipment Technology, School of Environmental Science
13 and Engineering, Nanjing University of Information Science and Technology,
14 Nanjing, Jiangsu, China

15 ²Atmospheric Sciences and Global Change Division, Pacific Northwest
16 National Laboratory, Richland, Washington, USA

17
18
19
20 *Correspondence to yang.yang@nuist.edu.cn

21 **Abstract**

22 Emissions of ozone (O₃) precursors in the United States have decreased
23 in recent decades, and near-surface O₃ concentrations showed a significant
24 decrease in summer but an increase in winter. In this study, an O₃ source
25 tagging technique is utilized in a chemistry-climate model to investigate the
26 source contributions to O₃ concentrations in the U.S. from various emitting
27 sectors and regions of nitrogen oxides (NO_x) and reactive carbon species
28 during 1995–2019. We show that domestic emission reductions from energy
29 and surface transportation are primarily responsible for the decrease in
30 summertime O₃ during 1995–2019. However, in winter the emission control also
31 weakens the NO_x titration process, resulting in considerable increases in O₃
32 levels from natural sources. Additionally, increases in aviation and shipping
33 activities and transpacific transport of O₃ from Asia largely contribute to the
34 winter O₃ increase. Changes in large-scale circulation also explain 15% of the
35 O₃ increasing trend.

36 **1. Introduction**

37 Ozone (O₃) near the surface has a significant impact on air quality and
38 public health (Haagen-Smit, 1952; Fleming et al., 2018). Since the increase in
39 anthropogenic emissions of O₃ precursors from preindustrial times, O₃ has now
40 become the third most important anthropogenic greenhouse gas in the
41 troposphere (Myhre et al., 2013). Major sources of O₃ in the troposphere
42 include the transport from the stratosphere and formation through
43 photochemical reactions within the troposphere involving two chemically
44 distinct groups of precursors: nitrogen oxides (NO_x) and reactive carbon
45 species, including carbon monoxide (CO), methane (CH₄), and non-methane
46 volatile organic compounds (NMVOCs) (Atkinson, 2000). O₃ precursors come
47 from a variety of sectors, and its relatively long lifetime of about 22 days
48 (Stevenson et al. 2006) favors the long-range transport of O₃. Due to the
49 nonlinearity of the O₃ production and its associated dependence on precursor
50 emissions (Seinfeld and Pandis, 1997), attributing O₃ pollution to its sources is
51 complicated.

52 Since the 1980s, O₃ precursor emissions have significantly reduced in the
53 United States (Duncan et al., 2016; Xing et al., 2013; Zhang et al., 2016; Zhang
54 et al., 2021). However, due to the nonlinear production chemistry of O₃,
55 complex seasonal meteorological influence, and long-range transport from
56 foreign source regions, domestic emissions reductions do not imply a decrease
57 in seasonal and annual O₃ concentrations. According to remote surface
58 measurements (Cooper et al., 2020) and aircraft observations (Gaudel et al.,
59 2020), the Sixth Assessment Report of the Intergovernmental Panel on Climate
60 Change (Szopa et al., 2021) showed a decreasing trend in annual mean O₃
61 concentrations in the western U.S. but an increasing trend in the eastern U.S.
62 since the mid-1990s. On the seasonal timescale, surface observations and
63 modeling results showed that O₃ concentrations over the U.S. had decreased

64 in summer due to the reductions in domestic anthropogenic emissions and
65 increased in winter related to the weakened NO_x titration since the late 1980s
66 (Cooper et al., 2012; Lin et al., 2017). It also shows that the increased
67 background O₃, especially due to an increased transport from Asia, can partly
68 offset the benefit of domestic emissions control over the western U.S. in
69 summer.

70 Source apportionment is a useful method for quantifying contributions to
71 air pollutants from specific source regions and/or sectors, which is beneficial to
72 emission control strategies (Yang et al., 2018). One method of obtaining an O₃
73 source-receptor relationship is to zero out or perturb emissions from a given
74 source region or sector in sensitivity simulations along with a baseline
75 simulation, which gives information about the response of O₃ to changes in
76 precursor emissions (e.g., Fiore et al., 2009; Hoor et al., 2009). However,
77 emission perturbation method requires many additional model simulations
78 when being used to estimate the contributions of multiple sources (Koo et al.,
79 2009; Wang et al., 2014) and the perturbation method may invalidate the
80 assumption of a linear relationship between the magnitude of the emission
81 perturbation and the magnitude of the O₃ change considering the nonlinearity
82 in O₃ chemistry, especially if large perturbations (e.g. zeroing out regional or
83 sector-wide emissions) are used. The tagging approach produces information
84 about the contribution of precursor emissions to the total amount of O₃ (Butler
85 et al., 2020). The perturbation and tagging methods are two different methods
86 answering different scientific questions, with the first for the impacts and the
87 last for the contributions (Grewe et al. 2010, Emmons et al. 2012, Clappier et
88 al. 2017 and Thunis et al., 2019). Both of these two methods can be used for
89 specific purpose to provide a comprehensive understanding source-receptor
90 relationships between precursor emissions and O₃ concentrations.

91 The source tagging method has been widely adopted in regional air quality

92 models to examine the O₃ attribution in the U.S., China, and/or Europe (Collet
93 et al., 2022; Gao et al., 2016; Lupaşcu and Butler, 2019). In some regional
94 models, O₃ apportionment is based on the ratio of chemical indicators to
95 determine the regime of O₃ generation (e.g., VOC-limited or NO_x-limited
96 regimes) and then attribute the generation of O₃ to the tag carried by a certain
97 precursor (VOCs or NO_x), which however cannot simultaneously attribute O₃
98 production to NO_x and VOCs, respectively (Dunker et al., 2002; Kwok et al.,
99 2015), while some models do not use the chemical indicators (Lupaşcu and
100 Butler, 2019; Mertens et al., 2020). In addition, due to the limitation in domain
101 size of regional air quality models, they are difficult to account for contributions
102 of intercontinental transport from several sources outside the model domain.
103 Recently, O₃ tagging techniques have been implemented in the global models
104 (e.g., Bates and Jacob, 2020; Han et al., 2018; Sudo and Akimoto, et al., 2007;
105 Zhang et al., 2008). However, in many global models, O₃ is tagged by the
106 production regions rather than the precursor emission regions, so that O₃ can
107 only be attributed to the area where O₃ is generated, rather than the source of
108 precursor emissions.

109 Here, based on a state-of-the-art tagging system implementation in a
110 global chemistry–climate model, the trends of near-surface O₃ concentrations
111 in the U.S. during 1995–2019 and the source attributions of the O₃ variations to
112 various emission sectors and regions of NO_x and reactive carbon species are
113 investigated in this study. Mechanisms of explaining the O₃ trends that involve
114 changes in anthropogenic emissions and large-scale circulations are also
115 explored.

116 **2. Methods**

117 **2.1 Model Description**

118 Tropospheric O₃ concentrations are simulated using the Community
119 Atmosphere Model version 4 with Chemistry (CAM4-chem) (Lamarque et al.,

120 2012; Tilmes et al., 2015), which is the atmospheric chemistry component of
121 the Community Earth System Model (CESM), at a horizontal resolution of 1.9°
122 latitude by 2.5° longitude with 26 vertical levels extending to 40 km above the
123 surface. The height of bottom layer near the surface is about 120 m and there
124 are about 4 layers under 2 km. The model configuration uses a comprehensive
125 tropospheric chemistry mechanism based on the Model for Ozone and Related
126 chemical Tracers version 4 (MOZART-4) (Emmons et al., 2010, 2012). Model
127 configurations simulate wet deposition of gas species using the Neu and
128 Prather (2012) scheme. Dry deposition is represented following the resistance
129 approach originally described in Wesely (1989). Stratosphere-troposphere
130 exchange of O₃ is treated by setting O₃ to stratospheric values as their
131 climatological means over 1996–2005 at the tropopause (Lamarque et al.,
132 2012), which is affected by atmospheric circulation and experiences the same
133 loss rates as O₃ in the troposphere (Tilmes et al., 2016). Sea surface
134 temperatures and sea ice concentrations in our simulations are prescribed at
135 present-day climatological conditions. The zonal and meridional wind fields are
136 nudged towards the MERRA-2 (Modern Era Retrospective-Analysis for
137 Research and Applications Version 2) reanalysis (Gelaro et al., 2017) at a 6-
138 hourly relaxation timescale in this study to better constrain large-scale
139 circulations by observations. The CAM4-chem performance in simulating
140 tropospheric O₃ and precursors has been fully evaluated in Tilmes et al. (2015).

141 **2.2 Ozone Source Tagging Technique**

142 The novel O₃ source tagging technique implemented in the model was
143 developed by Butler et al. (2018), which can provide a separate source
144 apportionment of tropospheric O₃ to the two distinct groups of precursor
145 emissions, i.e., NO_x and reactive carbon (CO, CH₄ and NMVOCs). The portion
146 of tropospheric O₃ that is attributable to the stratosphere-troposphere exchange
147 can also be quantified using this unique tagging technique. The source

148 attribution of O₃ requires two separate model runs with the tagging applied to
149 NO_x and reactive carbon species, respectively. Details of the O₃ tagging
150 technique are described in Butler et al. (2018).

151 In this study, near-surface O₃ is attributed to emission sectors and regions.
152 Emissions from individual sectors, including agriculture (AGR), energy (ENE),
153 industry (IND), residential, commercial and other (RCO), surface transportation
154 (TRA), waste management (WST), international shipping (SHP) and biomass
155 burning (BMB) emissions, as well as chemical production in the stratosphere
156 (STR) and extra chemical production (XTR, a small amount of O₃ produced due
157 to the self-reaction of OH radicals and the reactions of HO₂ with certain organic
158 peroxy radicals) are tagged for both NO_x and reactive carbon species. Aircraft
159 (AIR), soil (SOIL) and lightning (LGT) sources are separately tagged for NO_x
160 emissions, while solvents (SLV) and biogenic (BIO) sources are separately
161 tagged for NMVOCs emissions.

162 For the regional source attribution, we separately tag anthropogenic
163 sources from Africa (AFR), Central America (CAM), Europe (EUR), Middle East
164 (MDE), North America (NAM), East Asia (EAS), South Asia (SAS), Southeast
165 Asia (SEA) and rest of the world (ROW) (see Fig. 1 for the region map) and
166 natural sources (BMB, SOIL, LGT, BIO, STR and XTR). Additional tags for
167 methane (CH₄) and carbon monoxide (CO) are applied in both of the reactive
168 carbon tagging simulations that are used to attribute O₃ to emission sectors and
169 regions. We does not tag CH₄ by individual sources and its contribution is
170 lumped, because CH₄ is often considered separately from NMVOCs. It has a
171 relative long lifetime in the troposphere and it is well mixed in the troposphere
172 due to its exceptionally low reactivity, which can contribute to O₃ formation at
173 any location in the troposphere where photochemical conditions are favorable
174 (Fiore et al., 2008). CO also has a longer lifetime and lower reactivity than most
175 NMVOCs, separately tagging of CO is more conducive to distinguish its

176 contribution to O₃ from other NMVOCs. Therefore, the lumped total CO is
177 separately tagged in the sector attribution simulations, but the CO is not
178 specifically tagged in the regional attribution simulations due to the
179 computational limit.

180 **2.3 Emissions and Observation**

181 The global anthropogenic emissions, including NO_x, CO, NMVOCs, SO₂,
182 and NH₃, over 1990–2019 are from the Community Emissions Data System
183 (CEDS) version 20210205 (Hoesly et al., 2018) (See Figs. S1–S3). Biomass
184 burning emissions are obtained from the CMIP6 (Coupled Model
185 Intercomparison Project Phase 6) over 1990–2014 (van Marle et al., 2017) and
186 the emissions for the following five years (2015–2019) are interpolated from the
187 SSP2-4.5 forcing scenario (O'Neill et al., 2016). NO_x emitted from soils and
188 biogenic NMVOCs from vegetation are prescribed as in Tilmes et al. (2015) and
189 are kept at the present-day (2000) climatological levels during simulations.
190 Lightning emissions of NO_x are estimated using online parameterization based
191 on simulated cloud top heights from Price et al. (1997), which is scaled to
192 provide a global annual emission of 3–5 Tg N yr⁻¹ as Lamarque et. al. (2012).
193 CH₄ mixing ratio is fixed at a global average of 1750 parts per billion (ppb,
194 volume ratio in this study) during simulations.

195 Surface O₃ measurements in the U.S. are obtained from the U.S.
196 Environmental Protection Agency (EPA). Linear trends of surface O₃ are
197 calculated separately for boreal summer (June-July-August, JJA) and winter
198 (December-January-February, DJF). Seasonal mean for any site that has less
199 than 50% data availability in any month of a season is not calculated. O₃ trends
200 at sites is shown only when the data availability is greater than 85% during the
201 analyzed period.

202 **2.4 Experimental Design**

203 In this study, four groups of experiments are conducted, each group

204 includes both NO_x tagging simulation and reactive carbon tagging simulation.
205 Two BASE experiment groups include simulations with emission sectors and
206 regions, respectively, tagged for the two chemical distinct precursors. The
207 BASE experiments are performed with time-varying anthropogenic emissions
208 and winds nudged to MERRA-2 reanalysis. The other two groups of sensitivity
209 experiments (MET) are the same as BASE experiments, except that the
210 anthropogenic emissions are held at year 2019 level during simulations. All
211 experiments are performed over 1990–2019, with the first 5 years treated as
212 model spin-up and the last 25 years used for analysis. The BASE experiments
213 are analyzed to quantify the source attributions of O₃ in the U.S., unless stated
214 otherwise.

215 **2.5 Model Evaluation**

216 Figure S4 compares the simulated near-surface O₃ concentrations with
217 those from observations in 1995 and 2019, respectively. In general, the model
218 overestimates O₃ concentrations in the U.S. in both summer and winter by 10–
219 40%. It can capture the O₃ seasonality that high concentrations in summer and
220 low concentrations in winter. The spatial distributions can also be roughly
221 captured by the model, with statistically significant correlation coefficients
222 between simulations and observations in the range of 0.21–0.45. From 1995 to
223 2019, the O₃ concentrations in the U.S. decreased in summer and increased in
224 winter presented in observations. The model can produce the sign of the
225 changes, but has large biases in magnitudes, which will be discussed in the
226 following section.

227

228 **3 Results**

229 **3.1 Ground-level ozone trends in the U.S.**

230 Emissions of O₃ precursors have substantially reduced since 1995 in both
231 the western U.S. (WUS, 100–125°W, 30–45°N) and eastern U.S. (EUS, 70–

232 100°W, 30–45°N), primarily owing to the reductions in anthropogenic
233 emissions (Figs. S1–S3). However, the simulated annual near-surface O₃
234 concentrations present opposite trends between WUS and EUS, with increases
235 in EUS but weak decreases in WUS, which also exist in observations (Fig. 2a).

236 Looking at different seasons, we found the simulated contrasting trends in
237 annual mean O₃ concentrations between the WUS and EUS are dominated by
238 the strong decreases in O₃ concentrations in summer across the U.S. and
239 increased O₃ levels in winter over the central-eastern U.S. during 1995–2019.
240 The opposite trends between summer and winter have also been noted in many
241 previous studies (e.g., Copper et al., 2012; Lin et al., 2017, Jaffe et al., 2018).
242 The model reproduces the observed O₃ trend over EUS in summer and roughly
243 captures the O₃ trend over WUS in winter (Table S1). The decreasing trend over
244 WUS in summer and increasing trend over EUS in winter, however, are largely
245 overestimated in the model, partly attributed to the coarse model resolution.
246 The model also tends to overestimate the weakening of NO_x titration in winter,
247 leading to the biases. For spring and autumn, they are the transition between
248 summer and winter, having the similar spatial pattern of O₃ trends as annual
249 average, and will not be concerned in this study.

250 **3.2 Source attribution of ozone trends to emission sectors**

251 During 1995–2019, summer and winter NO_x emissions from energy and
252 surface transport sectors have significantly decreased in both WUS and EUS,
253 followed by industry and residential sectors, while those from aircraft have
254 increased slightly (Fig. 3). Emissions of NMVOCs from surface transportation,
255 solvents, industry, residential and waste sectors have decreased across the
256 U.S., while those from energy and agriculture have increased. CO emissions
257 have also significantly decreased over this time period.

258 The O₃ trends in the U.S. attributed to different emission source sectors
259 are shown in Fig. 5. The time series of the source contributions from NO_x and

260 reactive carbon emissions are shown in Figs. 4, respectively. In summer, the
261 O₃ attributed to energy and surface transportation NO_x emissions decreased at
262 the rate of 2.0±0.17 and 1.6±0.17 ppb/decade in WUS and 3.2±0.15 and
263 1.7±0.21 ppb/decade in EUS, respectively (Figs. 5a and 5c). On the contrary,
264 the O₃ contributed by aircraft NO_x emissions increased by 0.4±0.03 ppb/decade
265 in both WUS and EUS. Along with the reductions in anthropogenic emissions,
266 natural emissions are becoming increasingly important as sources for O₃
267 formation near the surface. Although NO_x emissions from soil are held at the
268 present-day climatological levels, they account for 0.7±0.08 and 1.7±0.10
269 ppb/decade increase in WUS and EUS, respectively, during 1995–2019, related
270 to the changing O₃ production efficiency under the more NO_x-sensitive
271 condition. Note that, during 1995–2019, the molar ratio (mol N /mol C) of
272 emitted NO_x to NMVOCs reduced from 0.11 to 0.07 in the WUS and from 0.14
273 to 0.07 in the EUS, confirming the enhanced NO_x-sensitive condition during the
274 analyzed time period. In recent decades, emissions from international shipping
275 have increased rapidly (Eyring, 2005; Müller-Casseres et al., 2021), but have
276 declined near the coast of the United States. Due to a strong chemical sink
277 associated with photolysis of O₃ with subsequent production of hydroxyl radical
278 (OH) from water vapor in summer (Johnson et al., 1999), the effect of increased
279 emissions of the far-shore ocean on the continental United States was blunted.
280 But the increase in shipping emissions inland tends to increase O₃
281 concentrations in eastern U.S. (Fig. S5).

282 In summer, biogenic sources dominate the emissions of NMVOCs in the
283 U.S. (Fig. S3). As the O₃ decreases, mainly due to the reductions in domestic
284 NO_x emissions, the contributions from biogenic emissions of NMVOCs have a
285 decreasing trend in the U.S. during 1995–2019 (Figs. 5b and 5d), even though
286 biogenic emissions were fixed during simulations. This also applies to CH₄, of
287 which the concentration was kept constant. This does not actually mean that

288 CH₄ and biogenic NMVOCs themselves contributed to the overall O₃ trend
289 through changing the precursor levels since they were kept constant during
290 simulations; rather, mainly due to the reductions in NO_x emissions, O₃
291 production efficiency by reactive carbon species decreases, leading to
292 decreasing trends of O₃ contribution by CH₄ and biogenic NMVOCs. In
293 conjunction with NO_x emission reductions, decreases in NMVOCs emissions
294 from surface transportation and industry sectors contribute negative O₃ trends
295 of -0.3 ± 0.0 and -0.1 ± 0.0 ppb/decade, respectively, in both WUS and EUS,
296 which are offset by the increases in NMVOCs emissions from energy and
297 agriculture sectors. Although the O₃ production efficiency of CO is relatively low,
298 the contributions of CO to O₃ concentrations largely decreased with trends of $-$
299 0.6 ± 0.1 and -0.5 ± 0.1 ppb/decade in WUS and EUS, respectively, due to the
300 massive reduction in anthropogenic emissions of CO (Fig. S1).

301 In winter, through the weakened NO_x titration process (Gao et al., 2013;
302 Simon et al., 2015), the NO_x emission control causes an increase in O₃ levels
303 during 1995–2019, especially the contribution from surface transportation
304 (0.4 ± 0.0 ppb/decade in WUS and 0.8 ± 0.1 ppb/decade in EUS) (Figs. 5e and
305 5g). Although aircraft NO_x emissions slightly increased, but O₃ attributed to
306 aircraft NO_x emissions shows positive trends as large as 0.4 ± 0.0 and 0.6 ± 0.0
307 ppb/decade in WUS and EUS, respectively. It is because aircraft emissions are
308 injected directly into the upper troposphere and lower stratosphere in a low
309 ambient NO_x condition and have a much higher O₃ enhancement efficiency
310 than surface emissions (Hodnebrog et al., 2011). It can be confirmed that the
311 NO_x from aircraft contributes to the increase in O₃ concentrations at 250 hPa in
312 high latitude regions of the Northern Hemisphere during 1995–2019 (Fig. S6).
313 The decrease in near-shore shipping weakened the NO_x titration, together with
314 the weakened O₃ chemical sink from water vapor in winter, leading to large
315 increasing trends of O₃ by 0.8 ± 0.1 and 1.0 ± 0.1 ppb/decade, respectively, in the

316 WUS and EUS during 1995–2019. Although most natural emissions do not
317 change during the simulations, the net O₃ chemical production is more sensitive
318 to NO_x under the emission control condition, resulting in the increasing O₃
319 trends contributed by the soil and lightning NO_x emissions. Due to the
320 weakened NO_x titration in winter, the contribution of stratospheric intrusion
321 increases at a rate of 0.6±0.1 and 1.0±0.1 ppb/decade over WUS and EUS,
322 respectively, when stratospheric contribution to the near-surface O₃ is relatively
323 high (Butler et al., 2018). Along with the weakened NO_x titration, contributions
324 from reactive carbon emissions to the near-surface O₃ in the U.S. also increase
325 for most species and sectors (Figs. 5f and 5h).

326 **3.3 Source attribution of ozone trends to emission regions**

327 The O₃ trends in the U.S. attributed to different emission source regions
328 are presented in Fig. 7. Time series of the source contributions are shown in
329 Figs. 6. In summer, domestic anthropogenic NO_x emissions (excluding those
330 from soil) within North America account for 49% of the near-surface O₃
331 concentration averaged over the U.S. (WUS+EUS) in 1995–2019. The
332 domestic emission reduction is the dominant factor causing the decline in
333 surface O₃ concentrations, with contributions of -4.4±0.22 and -5.7±0.3
334 ppb/decade to the trends over WUS and EUS, respectively, during 1995–2019
335 (Figs. 7a and 7c). Reductions in the NMVOCs emissions from North American
336 anthropogenic sources also decrease O₃ concentrations (Figs. 7b and 7d),
337 accompanying with the domestic NO_x emission control. The increase in NO_x
338 emissions from Asia contributes 0.7±0.1 ppb/decade to the total O₃ increasing
339 trend in WUS, partly offsetting the negative impact of domestic emission
340 reductions, but has a weak impact in EUS, which is consistent with previous
341 studies (Lin et al., 2017).

342 In winter, domestic anthropogenic NO_x emissions only account for 19% of
343 the surface O₃ concentration in the U.S. over 1995–2019, while NO_x sources

344 from lightning, rest of the world (mainly from the international shipping), and
345 Asia contribute 17%, 14%, and 11%, respectively, and O₃ from stratospheric
346 intrusion contributes 21% of the near-surface O₃ in the U.S. (Fig. 6). During
347 1995–2019, the significant increase in wintertime surface O₃ concentrations are
348 not directly linked to the reductions in domestic anthropogenic emissions (Figs.
349 7e and 7g). However, the domestic emission control weakens the NO_x titration,
350 resulting in considerable increases in O₃ originating from the natural sources,
351 including O₃ from stratospheric intrusion, lightning and soil emissions. The
352 natural sources combined contribute to positive O₃ trends of 1.2±0.2 and
353 2.4±0.3 ppb/decade in WUS and EUS, respectively. If the O₃ increase is
354 attributed to NMVOCs emissions, the combined natural source contribution is
355 even larger (1.4±0.2 and 2.5±0.2 ppb/decade) (Figs. 7f and 7h). O₃ produced
356 by CH₄ increases at rates of 1.3±0.1 and 2.1±0.1 ppb/decade in WUS and EUS,
357 respectively, due to the weakened NO_x titration. Increases in aviation and
358 shipping emissions explain the 1.2±0.1 and 1.5±0.1 ppb/decade of O₃ trends in
359 WUS and EUS, respectively (Figs. 5e and 5g). Long-range transport of O₃
360 produced from Asian NO_x emissions enhances the wintertime O₃ increasing
361 trends by 0.9±0.1 and 1.2±0.1 ppb/decade in WUS and EUS, respectively,
362 which are equally contributed by sources from East Asia, South Asia, and
363 Southeast Asia (Figs. 7e and 7g).

364 **3.4. Impact of variations in large-scale circulations on ozone trends**

365 Many studies have reported that O₃ spatial distribution is strongly
366 modulated by changes in large-scale circulations (e.g., Shen and Mickley, 2017;
367 Yang et al., 2014, 2022). Based on our MET experiments with anthropogenic
368 emissions kept unchanged, the changes in large-scale circulations show a
369 weak influence on the U.S. O₃ trends in summer (Fig. 8a) but cause a significant
370 O₃ rise in the central U.S. in winter (Fig. 8b). Averaged over the U.S., the near-
371 surface O₃ concentration in winter increases at the rate of 0.7±0.3 ppb/decade

372 during 1995–2019 in MET experiments, accounting for 15% of the trend of
373 4.7 ± 0.3 ppb/decade in BASE experiments. It suggests that the variation in
374 large-scale circulations is responsible for 15% of the increase in wintertime O₃
375 concentrations in the U.S. over 1995–2019. Variations in the circulation
376 facilitate O₃ transport from upper altitudes to the surface, as well as foreign
377 contributions from Asia, which is consistent with the finding in Lin et al. (2015).
378 The O₃ increasing trend in winter over the U.S. attributing to stratospheric
379 injection and Asian NO_x emissions due to dynamics are both 0.2 ± 0.1
380 ppb/decade (Fig. 8e). Therefore, changes in anthropogenic emissions are the
381 main factor affecting O₃ trends.

382 The changes in atmospheric circulation pattern support the above finding.
383 Compared to 1995–1999, anomalous northerly winds locate over high latitudes
384 of North America in 2015–2019 (Fig. 8c), strengthening the prevailing northerly
385 winds in winter. The strengthened winds transport O₃ from remote regions (e.g.,
386 Asia) to the central U.S. (Fig. 8g). In addition, an anomalous subsidence also
387 occurs over the central U.S. in 2015–2019, compared to 1995–1999 (Fig. 8d),
388 leading to an anomalous downward transport of O₃ from high altitudes and even
389 stratosphere to the surface (Figs. 8g and 8h). The horizontal and vertical
390 transport of O₃ together contribute to the near-surface O₃ increases in winter
391 during 1995–2019 associated with the changes in large-scale circulations. The
392 anomalous atmospheric circulation is likely linked to the location of the
393 midlatitude jet stream, which is influenced by ENSO cycle (Lin et al., 2015).

394

395 **4. Conclusions and discussions**

396 Using a global chemistry–climate model equipped with an O₃ source
397 tagging technique, we examine the long-term trends and source apportionment
398 of O₃ in the continental U.S. over 1995–2019 to various emission source
399 sectors and regions in this study. This model can capture the O₃ decreasing

400 trend over the EUS in summer and increasing trend over the WUS in winter
401 during this time period, but largely overestimates the decreasing trend over
402 WUS in summer and increasing trend over EUS in winter.

403 In summer, our simulation results show that the decline in surface O₃ is
404 dominated by the rapid reductions in NO_x emissions from energy and surface
405 transportation sectors, contributing to O₃ decreases at a rate of –2.0 and –1.6
406 ppb/decade in WUS and –3.2 and –1.7 ppb/decade in EUS, respectively. As
407 the anthropogenic NO_x decreases, the more NO_x-sensitive condition leads to a
408 positive O₃ trend of 0.7 and 1.7 ppb/decade in WUS and EUS, respectively,
409 contributed by the NO_x emissions from soil. Due to the reductions in NO_x
410 emissions, the O₃ production efficiency by reactive carbon species also
411 decreased, leading to the decreasing contributions to O₃ from reactive carbon
412 species in summer during 1995–2019. Even though biogenic NMVOCs
413 emissions and CH₄ mixing ratio were fixed during simulations, their
414 contributions also decreased related to the weakened O₃ production efficiency
415 by these precursors. Source region tagging suggests that the domestic
416 emission reductions are primarily responsible for the decreasing trend in
417 summertime near-surface O₃ concentrations in the U.S. during 1995–2019.

418 The mechanisms of wintertime O₃ increases over the U.S. are more
419 complex. First, the domestic emission control weakens the NO_x titration,
420 resulting in considerable increases in O₃ originating from natural sources,
421 including O₃ from stratospheric intrusion, lightning, soil and biogenic emissions.
422 The natural sources combined contribute a positive O₃ trend of more than 1 and
423 2 ppb/decade in WUS and EUS, respectively. Second, increases in aviation and
424 shipping emissions explain the 1.2 and 1.5 ppb/decade of O₃ trends in WUS
425 and EUS, respectively. Third, long-range transport of O₃ produced from Asian
426 NO_x emissions enhances the wintertime O₃ increasing trends by 0.9 and 1.2
427 ppb/decade in WUS and EUS, respectively. Fourth, the variation of horizontal

428 and vertical transport O₃ associated with the changes in large-scale circulation
429 contributes to the near-surface O₃ increases over the U.S. by 15% in winter
430 during 1995–2019. The overestimate of O₃ trend in the EUS might be related
431 to a potential biased model representation of vertical mixing in winter.
432 Compared to observations, the decreasing trend of O₃ concentrations over
433 WUS in summer and increasing trend over EUS in winter are overestimated in
434 the CAM4-chem model. Because most O₃ monitors are located in urban areas
435 and these areas generate strong O₃ during the day and have strong oxidation
436 titration at night, the daily and grid averaged O₃ concentrations output by the
437 model could be inconsistent with the urban observations. Besides, Lin et al.
438 (2017) found that the contribution from increasing Asian emissions offset that
439 from the U.S. emission reductions, resulting in a weak O₃ trend in WUS. In this
440 study, the Asian NO_x emissions only contribute to 0.6 ppb/decade of the total
441 positive trend in WUS in summer, much lower than the 3.7 ppb/decade
442 decrease attributable to the domestic emission reductions, suggesting that the
443 Asian contribution to the O₃ trends in WUS is likely underestimated in this study.
444 The bias of O₃ simulation in China may also lead to a bias in the wintertime O₃
445 trend over EUS. Additionally, international shipping can have a
446 disproportionately high influence on tropospheric O₃ due to the dispersed
447 nature of NO_x emissions (Butler et al., 2020; Kasibhatla et al., 2000; von Glasow
448 et al., 2003), together with the weakened NO_x titration, resulting in the
449 overestimation of O₃ trends. The fixed CH₄ mixing ratio during simulations also
450 biased the modeled O₃ trends in this study, which deserves further investigation
451 with the varying CH₄ levels in future studies. The coarse model resolution also
452 contributed to the biases. The overestimate of O₃ trend over EUS in winter,
453 likely related to the bias in NO_x titration, implies the overestimate of source
454 contributions to the trends in magnitude.

455 Compared with Butler et al. (2018), the simulation in this study shares

456 similar source sector contributions to the zonal average of O₃ concentrations at
457 the surface and 400 hPa in 2010 (Figs. S7 and S8 in this study and Figs. 5 and
458 6 in Butler et al. (2018)). The contributions from the stratosphere and lightning
459 NO_x are relatively higher in this study than Butler et al. (2018). This may be
460 related to the different anthropogenic emission inventories used, causing
461 different O₃ production/loss efficiencies by natural precursors. When comparing
462 the contributions from different source regions to surface O₃ concentrations in
463 North America, NO_x emissions from East Asia, South Asia, North America, and
464 Europe contributed 2.2, 1.1, 8.3, and 0.7 ppb of the surface O₃ in North America,
465 respectively (Fig. S9) in this study, which are also similar to those from Fig. 4 in
466 Butler et al. (2020). Both studies show the contributions of anthropogenic
467 NMVOCs to surface O₃ concentrations in North America are less than 10 ppb.

468 As the results of the study heavily depend on the emission inventory, here
469 the potential bias in emissions are also discussed. Compared with the previous
470 CEDS version used in this study (hereafter CEDS_{Hoesly}), the updated CEDS
471 inventory (hereafter CEDS_{GBD-MAPS}) (McDuffie et al., 2020) incorporates
472 updated activity data. For NO_x, the global emission from CEDS_{GBD-MAPS} is
473 smaller than that of CEDS_{Hoesly} after 2006 and shows a fast decreasing trend.
474 By 2014, global emission of NO_x is about 10 % lower than the CEDS_{Hoesly}
475 estimate. These differences are mainly reflected in the industrial and residential
476 sectors in China, followed by the transportation sector in India and Africa. For
477 global emission of NMVOCs, which remains relatively unchanged between the
478 CEDS_{Hoesly} and CEDS_{GBD-MAPS} inventories (Fig. 6 in McDuffie et al. 2020). The
479 global NO_x emission from EDGAR v4.3.2 inventory is less than CEDS_{Hoesly}
480 (Crippa et al., 2018). This difference in NO_x emissions may reduce O₃ trends in
481 U.S. from foreign contributions, especially from East Asia. Recent study also
482 reported a difference in NO_x emission distribution between CMIP5 and CMIP6
483 related to an error in data pre-processing in CEDS, leading to a northward shift

484 of O₃ burden in CMIP6 (Thor et al., 2023). The aviation emissions should be
485 corrected in future studies of O₃ simulations.
486

487 **Author contributions.** YY designed the research; PL and SL performed
488 simulations; PL analyzed the data. All authors including HW, KL, PW, BL, and
489 HL discussed the results and wrote the paper.

490

491 **Code and data availability.** The CESM is maintained by NCAR and is provided
492 freely to the community. The ozone tagging code has been described by Butler
493 et al. (2018). The MERRA-2 reanalysis data are from NASA GESDISC data
494 (<https://goldsmr5.gesdisc.eosdis.nasa.gov/data/MERRA2/M2I6NVANA.5.12.4/>,
495 last access: 1 August 2022). The surface O₃ measurements in U.S. are
496 obtained from the U.S. Environmental Protection Agency
497 (https://aqs.epa.gov/aqsweb/airdata/download_files.html#Daily, last access: 1
498 August 2022). The modeling results are made available at
499 <https://doi.org/10.5281/zenodo.6891316> (last access: 1 August 2022).

500

501 **Acknowledgments**

502 HW acknowledges the support by the U.S. Department of Energy (DOE), Office
503 of Science, Office of Biological and Environmental Research (BER), as part of
504 the Earth and Environmental System Modeling program. The Pacific Northwest
505 National Laboratory (PNNL) is operated for DOE by the Battelle Memorial
506 Institute under contract DE-AC05-76RLO1830.

507

508 **Financial support.** This study was supported by the National Key Research
509 and Development Program of China (grant 2020YFA0607803 and
510 2019YFA0606800), the National Natural Science Foundation of China (grant
511 41975159), and Jiangsu Science Fund for Distinguished Young Scholars (grant
512 BK20211541).

513

514 **Competing interests.** The authors declare that they have no conflict of interest.

515

516 **References**

517

518 Atkinson, R.: Atmospheric chemistry of VOCs and NO_x, *Atmos. Environ.*, 34,
519 2063-2101, [https://doi.org/10.1016/S1352-2310\(99\)00460-4](https://doi.org/10.1016/S1352-2310(99)00460-4), 2000.

520

521 Bates, K. H. and Jacob, D. J.: An Expanded Definition of the Odd Oxygen
522 Family for Tropospheric Ozone Budgets: Implications for Ozone Lifetime and
523 Stratospheric Influence, *Geophys. Res. Lett.*, 47, e2019GL084486,
524 <https://doi.org/10.1029/2019gl084486>, 2020.

525

526 Butler, T., Lupascu, A., and Nalam, A.: Attribution of ground-level ozone to
527 anthropogenic and natural sources of nitrogen oxides and reactive carbon in a
528 global chemical transport model, *Atmos. Chem. Phys.*, 20, 10707-10731,
529 <https://doi.org/10.5194/acp-20-10707-2020>, 2020.

530

531 Butler, T., Lupascu, A., Coates, J., and Zhu, a. S.: TOAST 1.0: Tropospheric
532 Ozone Attribution of Sources with Tagging for CESM 1.2.2, *Geosci. Model Dev.*,
533 <https://doi.org/10.5194/gmd-11-2825-2018>, 2018.

534

535 Castellanos, P. and Boersma, K. F.: Reductions in nitrogen oxides over Europe
536 driven by environmental policy and economic recession, *Sci. Rep.-UK*, 2, 265,
537 <https://doi.org/10.1038/srep00265>, 2012.

538

539 Collet, S., Kidokoro, T., Karamchandani, P., Jung, J., and Shah, T.: Future year
540 ozone source attribution modeling study using CMAQ-ISAM, *J&AWMA*, 68,
541 1239-1247 <https://doi.org/10.1080/10962247.2018.1496954>, 2018.

542

543 Cooper, O. R., Gao, R.-S., Tarasick, D., Leblanc, T., and Sweeney, C.: Long-
544 term ozone trends at rural ozone monitoring sites across the United States,
545 1990-2010, *J. Geophys. Res.: Atmospheres*, 117, D22307,
546 <https://doi.org/10.1029/2012JD018261>, 2012.

547

548 Cooper, O. R., Schultz, M. G., Schröder, S., Chang, K.-L., Gaudel, A., Gerardo,
549 Benítez, C., Cuevas, E., Fröhlich, M., Galbally, I. E., Kubistin, D., Lu, X., Audra,
550 McClure-Begley, A., Molloy, S., Nédélec, P., O'Brien, J., Oltmans, S. J., Irina,
551 Petropavlovskikh, I., Ries, L., Senik, I., Sjöberg, K., Solberg, S., Spain, T. G.,
552 Spangl, W., Steinbacher, M., Tarasick, D., Thouret, V., and Xu, X.: Multi-decadal
553 surface ozone trends at globally distributed remote locations, *Elem Sci Anth*, 8,
554 23, <https://doi.org/10.1525/elementa.420>, 2020.

555

556 Clappier, A., Belis, C. A., Pernigotti, D., and Thunis, P.: Source apportionment
557 and sensitivity analysis: two methodologies with two different purposes, *Geosci.*

558 Model Dev., 10, 4245–4256, <https://doi.org/10.5194/gmd-10-4245-2017>, 2017.
559

560 Crippa, M., Guizzardi, D., Muntean, M., Schaaf, E., Dentener, F., van Aardenne,
561 J. A., Monni, S., Doering, U., Olivier, J. G. J., Pagliari, V., and Janssens-
562 Maenhout, G.: Gridded emissions of air pollutants for the period 1970–2012
563 within EDGAR v4.3.2, *Earth Syst. Sci. Data*, 10, 1987–2013,
564 <https://doi.org/10.5194/essd-10-1987-2018>, 2018.
565

566 de Gouw, J. A., Parrish, D. D., Frost, G. J., and Trainer, M.: Reduced emissions
567 of CO₂, NO_x, and SO₂ from US power plants owing to switch from coal to
568 natural gas with combined cycle technology, *Earths Future*, 2, 75–82,
569 <https://doi.org/10.1002/2013EF000196>, 2014.
570

571 Duncan, B. N., Lamsal, L. N., Thompson, A. M., Yoshida, Y., Lu, Z., Streets, D.
572 G., Hurwitz, M. M., and Pickering, K. E.: A space-based, high-resolution view of
573 notable changes in urban NO_x pollution around the world (2005–2014), *J.*
574 *Geophys. Res.*, 21, 976-996, <https://doi.org/10.1002/2015JD024121>, 2016.
575

576 Duncan, B. N., Yoshida, Y., de Foy, B., Lamsal, L. N., Streets, D. G., Lu, Z.,
577 Pickering, K. E., and Krotkov, N. A.: The observed response of Ozone
578 Monitoring Instrument (OMI) NO₂ columns to NO_x emission controls on power
579 plants in the United States: 2005–2011, *Atmos. Environ.*, 81, 102–111,
580 <https://doi.org/10.1016/j.atmosenv.2013.08.068>, 2013.
581

582 Dunker, A. M., Yarwood, G., Ortman, J. P., and Wilson, G. M.: Comparison of
583 Source Apportionment and Source Sensitivity of Ozone in a Three-Dimensional
584 Air Quality Model, *Environ. Sci. Technol.*, 36, 2953–2964,
585 <https://doi.org/10.1021/es011418f>, 2002.
586

587 EIA: US Energy Information Administration: Drilling Productivity Report,
588 available at: <https://www.eia.gov/petroleum/drilling/>, last access: 7 April 2020.
589

590 Emmons, L. K., Hess, P. G., Lamarque, J.-F., and Pfister, G. G.: Tagged ozone
591 mechanism for MOZART-4, CAM-chem and other chemical transport models,
592 *Geosci. Model Dev.*, 5, 1531–1542, <https://doi.org/10.5194/gmd-5-1531-2012>,
593 2012.
594

595 Emmons, L. K., Walters, S., Hess, P. G., Lamarque, J.-F., Pfister, G. G., Fillmore,
596 D., Granier, C., Guenther, A., Kinnison, D., Laepple, T., Orlando, J., Tie, X.,
597 Tyndall, G., Wiedinmyer, C., Baughcum, S. L., and Kloster, S.: Description and
598 evaluation of the Model for Ozone and Related chemical Tracers, version 4
599 (MOZART-4), *Geosci. Model Dev.*, 3, 43–67, <https://doi.org/10.5194/gmd-3-43->

600 2010, 2010.
601
602 Eyring, V.: Emissions from international shipping: 1. The last 50 years, *J.*
603 *Geophys. Res.*, 110, <https://doi.org/10.1029/2004JD005619>, 2005.
604
605 Fiore, A. M., West, J. J., Horowitz, L. W., Naik, V., and Schwarzkopf, M. D.:
606 Characterizing the tropospheric ozone response to methane emission controls
607 and the benefits to climate and air quality, *J. Geophys. Res.*, 113, D08307,
608 <https://doi.org/10.1029/2007JD009162>, 2008.
609
610 Fiore, A. M., Dentener, F. J., Wild, O., Cuvelier, C., Schultz, M. G., Hess, P.,
611 Textor, C., Schulz, M., Doherty, R. M., Horowitz, L. W., MacKenzie, I. A.,
612 Sanderson, M. G., Shindell, D. T., Stevenson, D. S., Szopa, S., van Dingenen,
613 R., Zeng, G., Atherton, C., Bergmann, D., Bey, I., Carmichael, G., Collins, W. J.,
614 Duncan, B. N., Faluvegi, G., Folberth, G., Gauss, M., Gong, S., Hauglustaine,
615 D., Holloway, T., Isaksen, I. S. A., Jacob, D. J., Jonson, J. E., Kaminski, J. W.,
616 Keating, T. J., Lupu, A., Marmer, E., Montanaro, V., Park, R. J., Pitari, G., Pringle,
617 K. J., Pyle, J. A., Schroeder, S., Vivanco, M. G., Wind, P., Wojcik, G., Wu, S.,
618 and Zuber, A.: Multimodel estimates of intercontinental source-receptor
619 relationships for ozone pollution, *J. Geophys. Res.*, 114, D04301 ,
620 <https://doi.org/10.1029/2008JD010816>, 2009.
621
622 Fleming, Z. L., Doherty, R. M., Schneidemesser, E. V ., Malley, C. S., Cooper,
623 O. R., Pinto, J. P ., Colette, A., Xu, X., Simpson, D., Schultz, M. G., Lefohn, A.
624 S., Hamad, S., Moolla, R., Solberg, S., and Feng, Z.: Tropospheric Ozone
625 Assessment Report: Present-day ozone distribution and trends relevant to
626 human health, *Elem. Sci. Anth.*, 6, p. 12, <https://doi.org/10.1525/elementa.273>,
627 2018.
628
629 Gao, J., Zhu, B., Xiao, H., Kang, H., Hou, X., and Shao, P.: A case study of
630 surface ozone source apportionment during a high concentration episode,
631 under frequent shifting wind conditions over the Yangtze River Delta, China, *Sci.*
632 *Total Environ.*, 544, 853-863, <https://doi.org/10.1016/j.scitotenv.2015.12.039>,
633 2016.Gao, Y., Fu, J. S., Drake, J. B., Lamarque, J. F., and Liu, Y.: The impact
634 of emission and climate change on ozone in the United States under
635 representative concentration pathways (RCPs), *Atmos. Chem. Phys.*, 13, 9607-
636 9621, <https://doi.org/10.5194/acp-13-9607-2013>, 2013.
637
638 Gaudel, A., Cooper, O. R. , Chang, K. L., Bourgeois, I., Ziemke, J. R., Strode,
639 S. A., Oman, L. D., Sellitto, P., Nédélec, P., Bolt, R., Thouret, V. and Granier,C.:
640 Aircraft observations since the 1990s reveal increases of tropospheric ozone at
641 multiple locations across the Northern Hemisphere, *Sci. Advance.*, 6,

642 <https://doi.org/10.1126/sciadv.aba8272>, 2020.

643

644 Gelaro, R., McCarty, W., Suárez, M. J., Todling, R., Molod, A., Takacs, L.,
645 Randles, C. A., Darmenov, A., Bosilovich, M. G., Re-ichle, R., Wargan, K., Coy,
646 L., Cullather, R., Draper, C., Akella, S., Buchard, V., Conaty, A., da Silva, A. M.,
647 Gu, W., Kim, G., Koster, R., Lucchesi, R., Merkova, D., Nielsen, J. E., Partyka,
648 G., Pawson, S., Putman, W., Rienecker, M., Schubert, S. D., Sienkiewicz, M.,
649 and Zhao, B.: The Modern-Era Retrospective Analysis for Research and
650 Applications, Version 2 (MERRA-2), *J. Climate*, 30, 5419–5454,
651 <https://doi.org/10.1175/JCLI-D-16-0758.1>, 2017.

652

653 Haagen-Smit, A. J.: Chemistry and Physiology of Los Angeles Smog, *Ind. Eng.*
654 *Chem.*, 44, 1342-1346, <https://doi.org/10.1021/ie50510a045>, 1952.

655

656 Hodnebrog, Ø., Berntsen, T. K., Dessens, O., Gauss, M., Grewe, V., Isaksen, I.
657 S. A., Koffi, B., Myhre, G., Olivié, D., Prather, M. J., Pyle, J. A., Stordal, F., Szopa,
658 S., Tang, Q., van Velthoven, P., Williams, J. E., and Ødemark, K.: Future impact
659 of non-land based traffic emissions on atmospheric ozone and OH – an
660 optimistic scenario and a possible mitigation strategy, *Atmos. Chem. Phys.*, 11,
661 11293–11317, <https://doi.org/10.5194/acp-11-11293-2011>, 2011.

662

663 Hoesly, R. M., Smith, S. J., Feng, L., Klimont, Z., Janssens-Maenhout, G.,
664 Pitkanen, T., Seibert, J. J., Vu, L., Andres, R. J., Bolt, R. M., Bond, T. C.,
665 Dawidowski, L., Kholod, N., Kurokawa, J.-I., Li, M., Liu, L., Lu, Z., Moura, M. C.
666 P., O'Rourke, P. R., and Zhang, Q.: Historical (1750–2014) anthropogenic
667 emissions of reactive gases and aerosols from the Community Emissions Data
668 System (CEDS), *Geosci. Model Dev.*, 11, 369–408,
669 <https://doi.org/10.5194/gmd-11-369-2018>, 2018.

670

671 Han, H., Liu, J., Yuan, H., Zhuang, B., Zhu, Y., Wu, Y., Yan, Y., and Ding, A.:
672 Characteristics of intercontinental transport of tropospheric ozone from Africa
673 to Asia, *Atmos. Chem. Phys.*, 18, 4251–4276, [https://doi.org/10.5194/acp-18-](https://doi.org/10.5194/acp-18-4251-2018)
674 [4251-2018](https://doi.org/10.5194/acp-18-4251-2018), 2018.

675

676 Hoor, P., Borken-Kleefeld, J., Caro, D., Dessens, O., Endresen, Ø., Gauss, M.,
677 Grewe, V., Hauglustaine, D. A., Isaksen, I. S. A., Jöckel, P., Lelieveld, J., Myhre,
678 G., Meijer, E. W., Olivié, D., Prather, M. J., Poberaj, C. S., Shine, K. P., Staehelin,
679 J., Tang, Q., Aardenne, J. v., Velthoven, P. F. J. v., and Sausen, R.: The impact
680 of traffic emissions on atmospheric ozone and OH: results from QUANTIFY,
681 *Atmos. Chem. Phys.*, 9, 3113-3116, <https://doi.org/10.5194/acp-9-3113-2009>,
682 2009.

683

684 Jaffe, D. A., Cooper, O. R., Fiore, A. M., Henderson, B. H., Tonnesen, G. S.,
685 Russell, A. G., Henze, D. K., Langford, A. O., Lin, M., and Moore, T.: Scientific
686 assessment of background ozone over the U.S.: Implications for air quality
687 management, *Elem. Sci. Anth*, 6, 56, doi: <https://doi.org/10.1525/elementa.309>,
688 2018.

689

690 Johnson, C., Collins, W., Stevenson, D., and Derwent, R.: Relative roles of
691 climate and emissions changes on future tropospheric oxidant concentrations,
692 *J. Geophys. Res.-Atmos.*, 104, 18631–18645,
693 <https://doi.org/10.1029/1999JD900204>, 1999.

694

695 Kasibhatla, P., Levy, H., Moxim, W. J., Pandis, S. N., Corbett, J. J., Peterson,
696 M. C., Honrath, R. E., Frost, G. J., Knapp, K., Parrish, D. D., and Ryerson, T.
697 B.: Do emissions from ships have a significant impact on concentrations of
698 nitrogen oxides in the marine boundary layer?, *Geophys. Res. Lett.*, 27, 2229–
699 2232, <https://doi.org/10.1029/2000gl011387>, 2000.

700

701 Koo, B., Wilson, G. M., Morris, R., Dunker, A. M., and Yarwood, G.: Comparison
702 of Source Apportionment and Sensitivity Analysis in a Particulate Matter Air
703 Quality Model, *Environ. Sci. Technol.*, 43, 6669–6675,
704 <https://doi.org/10.1021/es9008129>, 2009.

705

706 Krotkov, N. A., McLinden, C. A., Li, C., Lamsal, L. N., Celarier, E. A., Marchenko,
707 S. V., Swartz, W. H., Bucsela, E. J., Joiner, J., Duncan, B. N., Boersma, K. F.,
708 Veefkind, J. P., Levelt, P. F., Fioletov, V. E., Dickerson, R. R., He, H., Lu, Z.,
709 and Streets, D. G.: Aura OMI observations of regional SO₂ and NO₂ pollution
710 changes from 2005 to 2015, *Atmos. Chem. Phys.*, 16, 4605–4629,
711 <https://doi.org/10.5194/acp-16-4605-2016>, 2016.

712

713 Kwok, R. H. F., Baker, K. R., Napelenok, S. L., and Tonnesen, G. S.:
714 Photochemical grid model implementation and application of VOC, NO_x, and
715 O₃ source apportionment, *Geosci. Model Dev.*, 8, 99–114,
716 <https://doi.org/10.5194/gmd-8-99-2015>, 2015.

717

718 Lamarque, J.-F., Emmons, L. K., Hess, P. G., Kinnison, D. E., Tilmes, S., Vitt,
719 F., Heald, C. L., Holland, E. A., Lauritzen, P. H., Neu, J., Orlando, J. J., Rasch,
720 P. J., and Tyndall, G. K.: CAM-chem: description and evaluation of interactive
721 atmospheric chemistry in the Community Earth System Model, *Geosci. Model*
722 *Dev.*, 5, 369–411, <https://doi.org/10.5194/gmd-5-369-2012>, 2012.

723

724 Lin, M., Fiore, A. M., Horowitz, L. W., Langford, A. O., Oltmans, S. J., Tarasick,
725 D., and Rieder, H. E.: Climate variability modulates western U.S. ozone air

726 quality in spring via deep stratospheric intrusions, *Nat. Commun.*, 6, 7105,
727 <https://doi.org/10.1038/ncomms8105>, 2015.

728

729 Lin, M., Horowitz, L. W., Payton, R., Fiore, A. M., and Tonnesen, G. S.: US
730 surface ozone trends and extremes from 1980 to 2014: quantifying the roles of
731 rising Asian emissions, domestic controls, wildfires, and climate, *Atmos. Chem.*
732 *Phys.*, 17, 2943–2970, <https://doi.org/10.5194/acp-17-2943-2017>, 2017.

733

734 Lin, M., Fiore, A. M., Cooper, O. R., Horowitz, L. W., Langford, A. O., Levy, H.,
735 Johnson, B. J., Naik, V., Oltmans, S. J., and Senff, C. J.: Springtime high
736 surface ozone events over the western United States: Quantifying the role of
737 stratospheric intrusions, *J. Geophys. Res. Atmos.*, 117,
738 <https://doi.org/10.1029/2012JD018151>, 2012.

739

740 Lupaşcu, A. and Butler, T.: Source attribution of European surface O₃ using a
741 tagged O₃ mechanism, *Atmos. Chem. Phys.*, 19, 14535–14558,
742 <https://doi.org/10.5194/acp-19-14535-2019>, 2019.

743

744 Mertens, M., Kerkweg, A., Grewe, V., Jöckel, P., and Sausen, R.: Attributing
745 ozone and its precursors to land transport emissions in Europe and Germany,
746 *Atmos. Chem. Phys.*, 20, 7843–7873, [https://doi.org/10.5194/acp-20-7843-](https://doi.org/10.5194/acp-20-7843-2020)
747 2020, 2020.

748

749 McDuffie, E. E., Smith, S. J., O'Rourke, P., Tibrewal, K., Venkataraman, C.,
750 Marais, E. A., Zheng, B., Crippa, M., Brauer, M., and Martin, R. V.: A global
751 anthropogenic emission inventory of atmospheric pollutants from sector- and
752 fuel-specific sources (1970–2017): an application of the Community Emissions
753 Data System (CEDS), *Earth Syst. Sci. Data*, 12, 3413–3442,
754 <https://doi.org/10.5194/essd-12-3413-2020>, 2020.

755

756 Müller-Casseres, E., Edelenbosch, O. Y., Szklo, A., Schaeffer, R., and van
757 Vuuren, D. P.: Global futures of trade impacting the challenge to decarbonize
758 the international shipping sector, *Energy*, 237, 121547,
759 <https://doi.org/10.1016/j.energy.2021.121547>, 2021

760

761 Myhre, G., D. Shindell, F.-M. Bréon, W. Collins, J. Fuglestedt, J. Huang, D.
762 Koch, J.-F. Lamarque, D. Lee, B. Mendoza, T. Nakajima, A. Robock, G.
763 Stephens, T. Takemura and H. Zhang, 2013: Anthropogenic and Natural
764 Radiative Forcing. In: *Climate Change 2013: The Physical Science Basis.*
765 Contribution of Working Group I to the Fifth Assessment Report of the
766 Intergovernmental Panel on Climate Change [Stocker, T.F., D. Qin, G.-K.
767 Plattner, M. Tignor, S.K. Allen, J. Boschung, A. Nauels, Y. Xia, V. Bex and P.M.

768 Midgley (eds.)). Cambridge University Press, Cambridge, United Kingdom and
769 New York, NY, USA, 2013.
770
771 O'Neill, B. C., Tebaldi, C., van Vuuren, D. P., Eyring, V., Friedlingstein, P., Hurtt,
772 G., Knutti, R., Kriegler, E., Lamarque, J.-F., Lowe, J., Meehl, G. A., Moss, R.,
773 Riahi, K., and Sanderson, B. M.: The Scenario Model Intercomparison Project
774 (ScenarioMIP) for CMIP6, *Geosci. Model Dev.*, 9, 3461-3482,
775 <https://doi.org/10.5194/gmd-9-3461-2016>, 2016.
776
777 Price, C., Penner, J., and Prather, M.: NO_x from lightning 1, Global distribution
778 based on lightning physics, *J. Geophys. Res.*, 102, 5929–5941,
779 <https://doi.org/10.1029/96JD03504>, 1997.
780
781 Seinfeld, J. H. and Pandis, S. N.: *Atmospheric Chemistry and Physics: From*
782 *Air Pollution to Climate Change*, J. Wiley, Hoboken, N.J., 2006.
783
784 Simon, H., Reff, A., Wells, B., Xing, J., and Frank, N.: Ozone trends across the
785 United States over a period of decreasing NO_x and VOC emissions, *Environ.*
786 *Sci. Technol.*, 49, 186-195, <https://doi.org/10.1021/es504514z>, 2015.
787
788 Shen, L. and Mickley, L. J.: Effects of El Niño on summertime ozone air quality
789 in the eastern United States *Geophys. Res. Lett.* 44, 12543–50,
790 <https://doi.org/10.1002/2017GL076150>, 2017.
791
792 Stevenson, D. S., Dentener, F. J., Schultz, M. G., Ellingsen, K., van Noije, T. P.
793 C., Wild, O., Zeng, G., Amann, M., Atherton, C. S., Bell, N., Bergmann, D. J.,
794 Bey, I., Butler, T., Cofala, J., Collins, W. J., Derwent, R. G., Doherty, R. M.,
795 Drevet, J., Eskes, H. J., Fiore, A. M., Gauss, M., Hauglustaine, D. A., Horowitz,
796 L. W., Isaksen, I. S. A., Krol, M. C., Lamarque, J.-F., Lawrence, M. G.,
797 Montanaro, V., Müller, J.-F., Pitari, G., Prather, M. J., Pyle, J. A., Rast, S.,
798 Rodriguez, J. M., Sanderson, M. G., Savage, N. H., Shindell, D. T., Strahan, S.
799 E., Sudo, K., and Szopa, S.: Multimodel ensemble simulations of present-day
800 and near-future tropospheric ozone. *J. Geophys. Res.*, 111, D08301.
801 <https://doi.org/10.1029/2005JD006338>, 2006.
802
803 Sudo, K., and Akimoto, H.: Global source attribution of tropospheric ozone:
804 Long-range transport from various source regions, *J. Geophys. Res.*, 112,
805 D12302, <https://doi.org/10.1029/2006JD007992>, 2007.
806
807 Szopa, S., V. Naik, B. Adhikary, P. Artaxo, T. Berntsen, W.D. Collins, S. Fuzzi,
808 L. Gallardo, A. Kiendler-Scharr, Z. Klimont, H. Liao, N. Unger, and P. Zanis:
809 Short-Lived Climate Forcers. In *Climate Change 2021: The Physical Science*

810 Basis. Contribution of Working Group I to the Sixth Assessment Report of the
811 Intergovernmental Panel on Climate Change [Masson-Delmotte, V., P. Zhai,
812 A. Pirani, S.L. Connors, C. Péan, S. Berger, N. Caud, Y. Chen, L. Goldfarb,
813 M.I. Gomis, M. Huang, K. Leitzell, E. Lonnoy, J.B.R. Matthews, T.K.
814 Maycock, T. Waterfield, O. Yelekçi, R. Yu, and B. Zhou (eds.)]. Cambridge
815 University Press, Cambridge, United Kingdom and New York, NY, USA, pp.
816 817–922, <https://doi.org/10.1017/9781009157896.008>, 2021.

817

818 Thor, R. N., Mertens, M., Matthes, S., Righi, M., Hendricks, J., Brinkop, S., Graf,
819 P., Grewe, V., Jöckel, P., and Smith, S.: An inconsistency in aviation emissions
820 between CMIP5 and CMIP6 and the implications for short-lived species and
821 their radiative forcing, *Geosci. Model Dev.*, 16, 1459–1466,
822 <https://doi.org/10.5194/gmd-16-1459-2023>, 2023.

823

824 Thunis, P., Clappier, A., Tarrason, L., Cuvelier, C., Monteiro, A., Pisoni, E.,
825 Wesseling, J., Belis, C., Pirovano, G., Janssen, S., Guerreiro, C., and Peduzzi,
826 E.: Source apportionment to support air quality planning: Strengths and
827 weaknesses of existing approaches, *Environ. Int.*, 130, 104825,
828 <https://doi.org/10.1016/j.envint.2019.05.019>, 2019.

829

830 Tilmes, S., Lamarque, J. F., Emmons, L. K., Kinnison, D. E., Marsh, D., Garcia,
831 R. R., Smith, A. K., Neely, R. R., Conley, A., Vitt, F., Val Martin, M., Tanimoto,
832 H., Simpson, I., Blake, D. R., and Blake, N.: Representation of the Community
833 Earth System Model (CESM1) CAM4-chem within the Chemistry-Climate
834 Model Initiative (CCMI), *Geosci. Model Dev.*, 9, 1853–1890,
835 <https://doi.org/10.5194/gmd-9-1853-2016>, 2016.

836

837 Tilmes, S., Lamarque, J. F., Emmons, L. K., Kinnison, D. E., Ma, P. L., Liu, X.,
838 Ghan, S., Bardeen, C., Arnold, S., Deeter, M., Vitt, F., Ryerson, T., Elkins, J. W.,
839 Moore, F., Spackman, J. R., and Val Martin, M.: Description and evaluation of
840 tropospheric chemistry and aerosols in the Community Earth System Model
841 (CESM1.2), *Geosci. Model Dev.*, 8, 1395–1426, [https://doi.org/10.5194/gmd-8-](https://doi.org/10.5194/gmd-8-1395-2015)
842 1395-2015, 2015.

843

844 Tilmes, S., Lamarque, J. F., Emmons, L. K., Kinnison, D. E., Ma, P. L., Liu, X.,
845 Ghan, S., Bardeen, C., Arnold, S., Deeter, M., Vitt, F., Ryerson, T., Elkins, J. W.,
846 Moore, F., Spackman, J. R., and Val Martin, M.: Description and evaluation of
847 tropospheric chemistry and aerosols in the Community Earth System Model
848 (CESM1.2), *Geosci. Model Dev.*, 8, 1395–1426, [https://doi.org/10.5194/gmd-8-](https://doi.org/10.5194/gmd-8-1395-2015)
849 1395-2015, 2015.

850

851 van Marle, M. J. E., Kloster, S., Magi, B. I., Marlon, J. R., Daniau, A.-L., Field,

852 R. D., Arneth, A., Forrest, M., Hantson, S., Kehrwald, N. M., Knorr, W., Lasslop,
853 G., Li, F., Mangeon, S., Yue, C., Kaiser, J. W., and van der Werf, G. R.: Historic
854 global biomass burning emissions for CMIP6 (BB4CMIP) based on merging
855 satellite observations with proxies and fire models (1750–2015), *Geosci. Model*
856 *Dev.*, 10, 3329–3357, <https://doi.org/10.5194/gmd-10-3329-2017>, 2017.

857

858 von Glasow, R., Lawrence, M. G., Sander, R., and Crutzen, P. J.: Modeling the
859 chemical effects of ship exhaust in the cloudfree marine boundary layer, *Atmos.*
860 *Chem. Phys.*, 3, 233–250, <https://doi.org/10.5194/acp-3-233-2003>, 2003.

861

862 Wang, H., Rasch, P. J., Easter, R. C., Singh, B., Zhang, R., Ma, P.-L., Qian, Y.,
863 Ghan, S. J., and Beagley, N.: Using an explicit emission tagging method in
864 global modeling of source-receptor relationships for black carbon in the Arctic:
865 Variations, sources, and transport pathways, *J. Geophys. Res.*, 119, 12888–
866 12909, <https://doi.org/10.1002/2014JD022297>, 2014.

867

868 Wesely, M. L.: Parameterizations for surface resistance to gaseous dry
869 deposition in regional-scale numerical models, *Atmos. Environ.*, 23, 1293–1304,
870 [https://doi.org/10.1016/0004-6981\(89\)90153-4](https://doi.org/10.1016/0004-6981(89)90153-4), 1989.

871

872 Xing, J., Pleim, J. E., Mathur, R., Pouliot, G., Hogrefe, C., Gan, C.-M., and Wei,
873 C.: Historical gaseous and primary aerosol emissions in the United States from
874 1990 to 2010, *Atmos. Chem. Phys.*, 13, 7531–7549,
875 <https://doi.org/10.5194/acp-13-7531-2013>, 2013.

876

877 Yang, Y., Li, M., Wang, H., Li, H., Wang, P., Li, K., Gao, M., and Liao, H.: ENSO
878 modulation of summertime tropospheric ozone over China, *Environ. Res. Lett.*,
879 17, 034020, <https://doi.org/10.1088/1748-9326/ac54cd>, 2022.

880

881 Yang, Y., Liao, H., and Li, J.: Impacts of the East Asian summer monsoon on
882 interannual variations of summertime surface-layer ozone concentrations over
883 China, *Atmos. Chem. Phys.*, 14, 6867–6879, [https://doi.org/10.5194/acp-14-](https://doi.org/10.5194/acp-14-6867-2014)
884 [6867-2014](https://doi.org/10.5194/acp-14-6867-2014), 2014.

885

886 Yang, Y., Wang, H., Smith, S. J., Zhang, R., Lou, S., Yu, H., Li, C., and Rasch,
887 P. J.: Source apportionments of aerosols and their direct radiative forcing and
888 long-term trends over continental United States, *Earth's Future*, 6, 793–808,
889 <https://doi.org/10.1029/2018EF000859>, 2018.

890

891 Zhang, L., Jacob, D. J., Boersma, K. F., Jaffe, D. A., Olson, J. R., Bowman, K.
892 W., Worden, J. R., Thompson, A. M., Avery, M. A., Cohen, R. C., Dibb, J. E.,
893 Flock, F. M., Fuelberg, H. E., Huey, L. G., McMillan, W. W., Singh, H. B., and

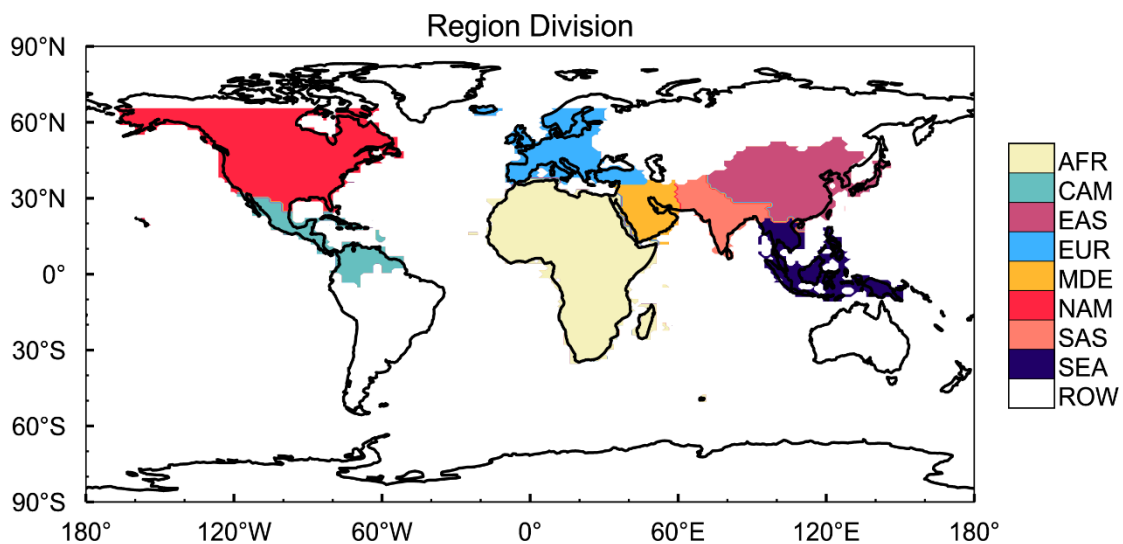
894 Weinheimer, A. J.: Transpacific transport of ozone pollution and the effect of
895 recent Asian emission increases on air quality in North America: an integrated
896 analysis using satellite, aircraft, ozonesonde, and surface observations, *Atmos.*
897 *Chem. Phys.*, 8, 6117–6136, <https://doi.org/10.5194/acp-8-6117-2008>, 2008.

898

899 Zhang, Y., Cooper, O. R., Gaudel, A., Nédélec, P., Ogino, S. Y., Thompson, A.
900 M., and West, J. J.: Tropospheric ozone change from 1980 to 2010 dominated
901 by equatorward redistribution of emissions, *Nat. Geosci.*, 9, 875-879,
902 <https://doi.org/10.1038/ngeo2827>, 2016.

903

904 Zhang, Y., West, J. J., Emmons, L. K., Flemming, J., Jonson, J. E., Lund, M. T.,
905 Sekiya, T., Sudo, K., Gaudel, A., Chang, K. L., Nédélec, P., and Thouret, V.:
906 Contributions of World Regions to the Global Tropospheric Ozone Burden
907 Change From 1980 to 2010, *Geophys. Res. Lett.*, 48,
908 <https://doi.org/10.1029/2020GL089184>, 2021.

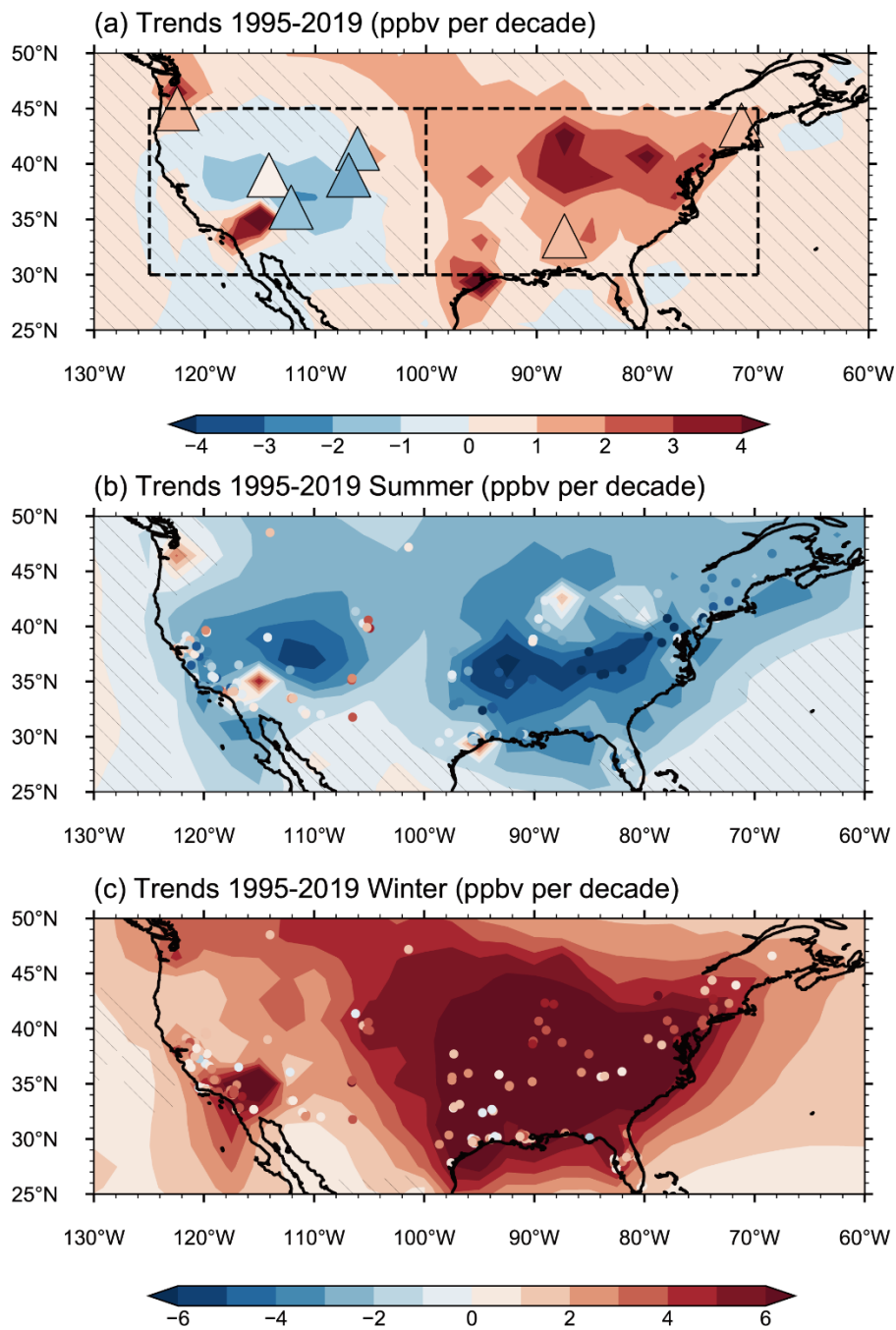


909

910

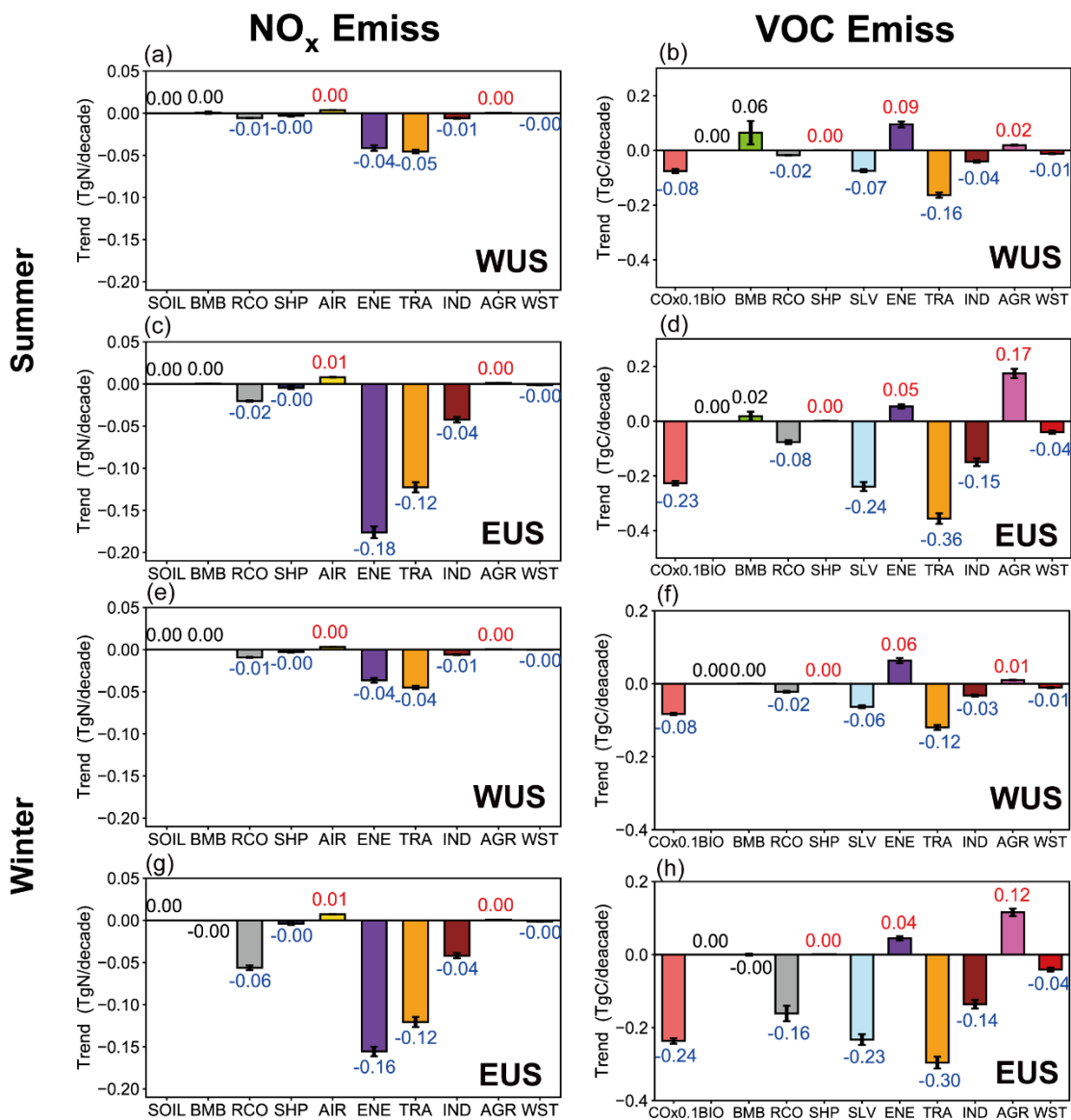
911 **Figure 1.** Source regions that are selected for O₃ source tagging in this study,
 912 include Africa (AFR), Central America (CAM), East Asia (EAS), Europe (EUR),
 913 Middle East (MDE), North America (NAM), South Asia (SAS), Southeast Asia
 914 (SEA) and rest of the world (ROW).

915



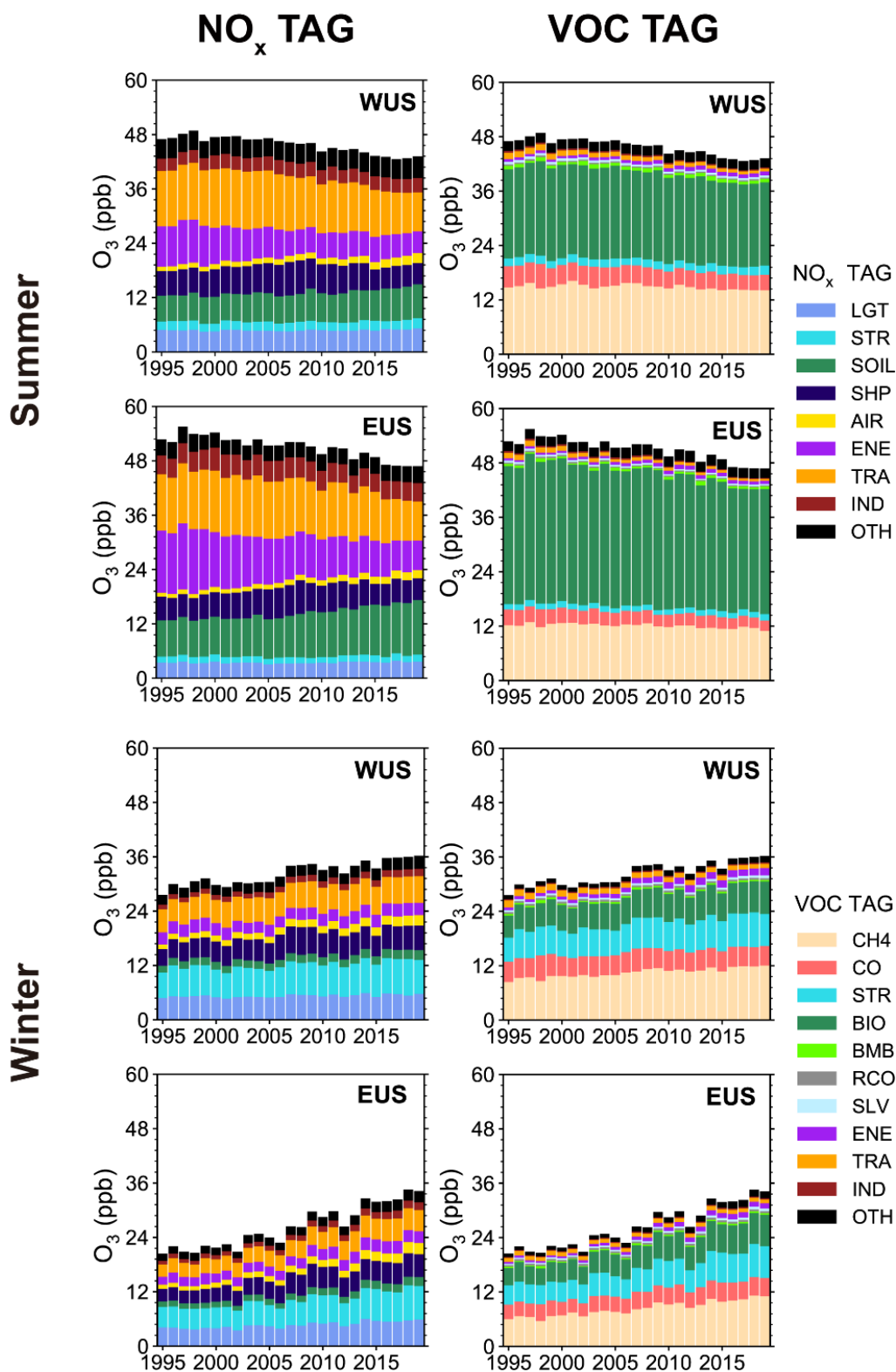
916
 917
 918
 919
 920
 921
 922
 923
 924
 925
 926
 927

Figure 2. Linear trends (ppb/decade) of simulated (contours) and observed (color-filled markers) (a) annual, (b) JJA and (c) DJF mean near-surface O₃ concentrations during 1995–2019. Areas without hatches indicate statistical significance with 95% confidence. The boxes in (a) mark the western U.S. (WUS, 100–125°W, 30–45°N) and eastern U.S. (EUS, 70–100°W, 30–45°N), respectively. The observed annual O₃ concentration trends in (a) are derived from IPCC AR6, based on Cooper et al. (2020) and Gaudel et al. (2020) over 1995–2017. The observed seasonal O₃ concentration trends in (b) and (c) are calculated based on the U.S. EPA O₃ measurements over 1995–2019.



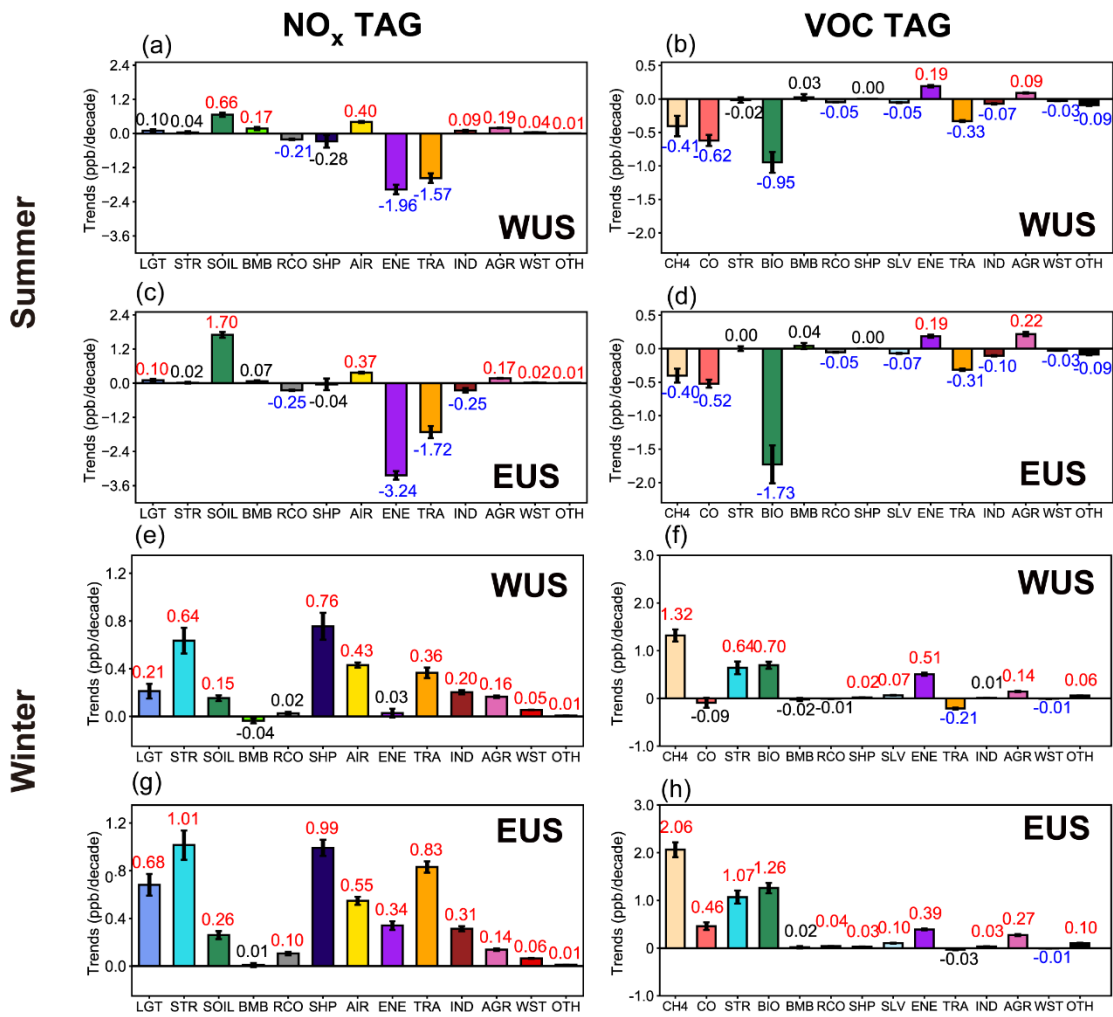
928

929 **Figure 3.** Linear trends of NO_x and reactive carbon emissions from various
 930 sectors in summer and winter over WUS and EUS. The increasing and
 931 decreasing trends marked with red and blue values, respectively, indicate
 932 statistical significance with 95% confidence.



933
 934
 935
 936
 937
 938

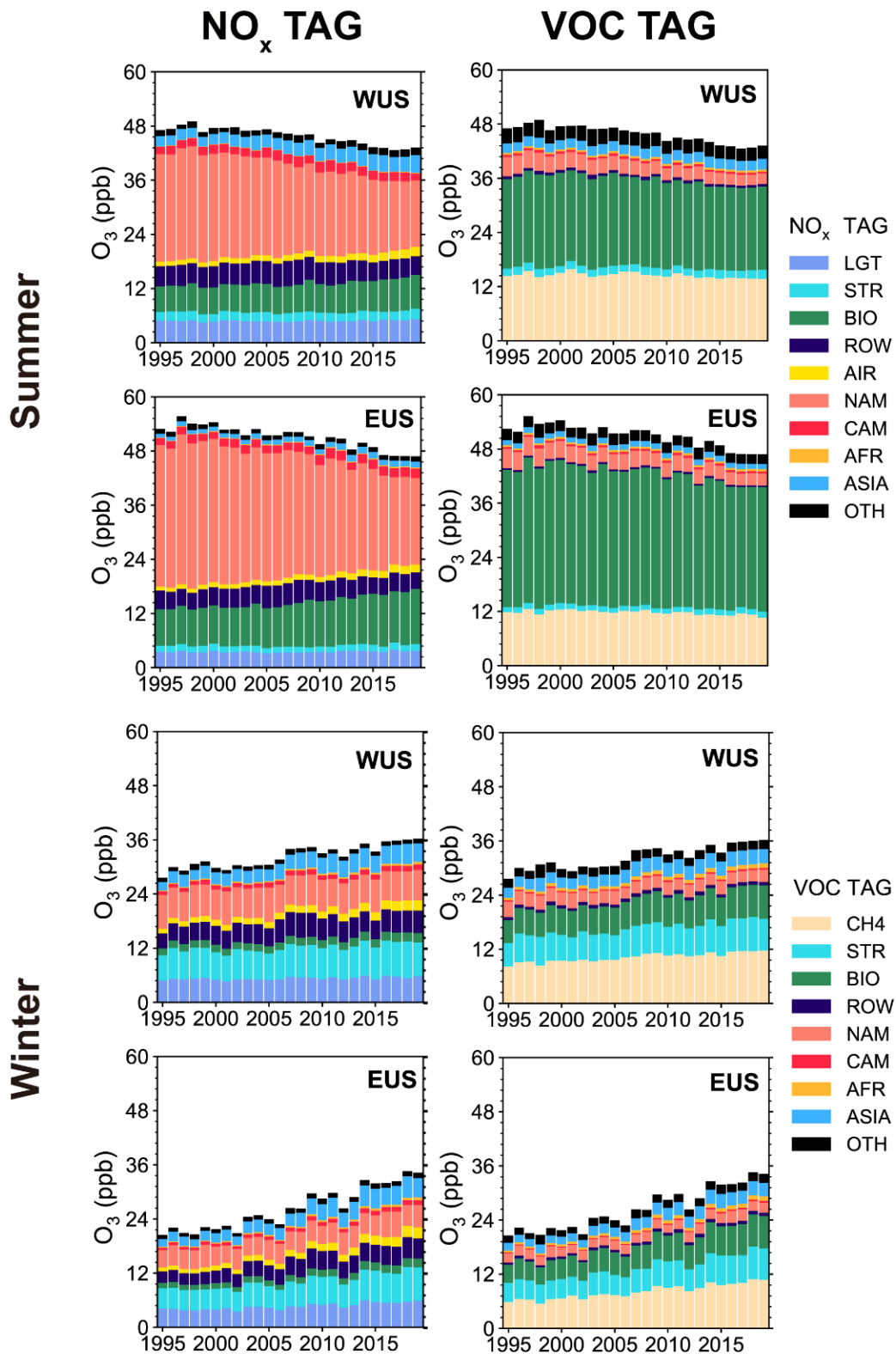
Figure 4. Time series of near-surface O₃ concentrations (ppb) averaged over WUS and EUS contributed by NO_x and reactive carbon emissions from different sectors in summer and winter during 1995–2019. Sources with small contributions are combined and shown as OTH.



939

940

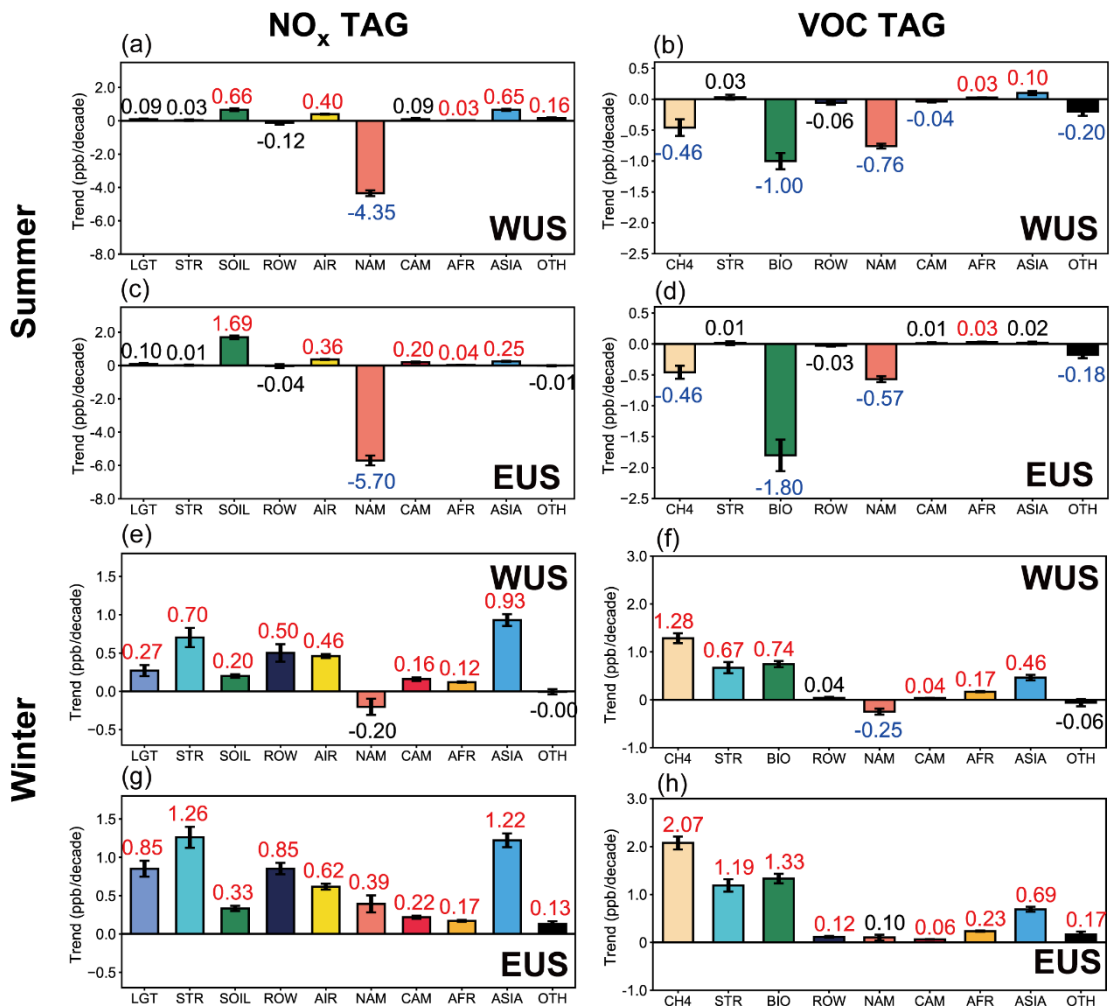
941 **Figure 5.** Linear trends (ppb/decade) of near-surface O₃ concentrations in
 942 summer and winter over WUS and EUS contributed by the NO_x (left) and
 943 reactive carbon (right) emissions from various sectors (color bars). The
 944 increasing and decreasing trends marked with red and blue color numbers,
 945 respectively, indicate statistical significance with 95% confidence. Other
 946 sources having small contributions are combined and shown as OTH.



947

948

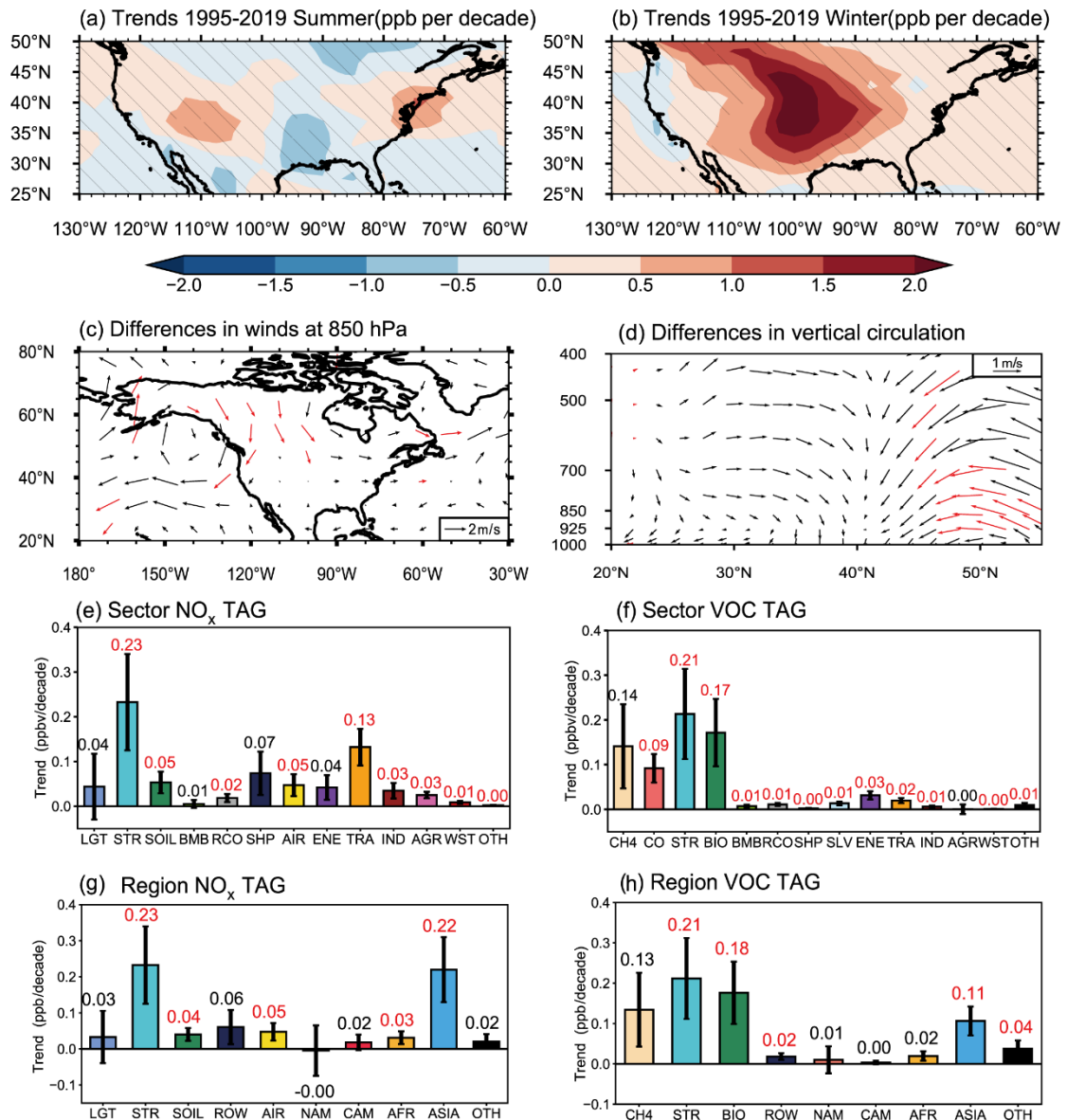
949 **Figure 6.** Time series of near-surface O₃ concentrations (ppb) averaged over
 950 WUS and EUS contributed by NO_x and reactive carbon emissions from different
 951 source regions in summer and winter during 1995–2019. Sources with small
 952 contributions are combined and shown as OTH.



953

954

955 **Figure 7.** Linear trends (ppb/decade) of near-surface O₃ concentrations in
 956 summer and winter over WUS and EUS contributed by the NO_x (left) and
 957 reactive carbon (right) emissions from various source regions (color bars). The
 958 increasing and decreasing trends marked with red and blue color numbers,
 959 respectively, indicate statistical significance with 95% confidence. Contributions
 960 from source regions EAS, SAS and SEA are combined to ASIA. Other sources
 961 having small contributions are combined and shown as OTH.



962
963

964 **Figure 8.** Linear trends (ppb/decade) of simulated (a) JJA and (b) DJF mean
965 near-surface O₃ concentrations during 1995–2019. Differences between the
966 first (1995–1999) and last (2015–2019) five years during 1995–2019 (last–
967 first) in DJF mean (c) 850 hPa horizontal winds and (d) meridional winds and
968 vertical velocity averaged over 90–105°W. Areas without hatches in (a) and
969 (b) and red arrows in (c) and (d) indicate statistical significance with 95%
970 confidence. All results are from the MET experiments. Linear trends
971 (ppb/decade) of near-surface O₃ concentrations in winter over the U.S.,
972 contributed by the NO_x (e, g) and reactive carbon (f, h) emissions from various
973 source sectors (e, f) and regions (g, h). The increasing and decreasing trends
974 marked with red and blue color numbers, respectively, indicate statistical
975 significance with 95% confidence. Contributions from source regions EAS,
976 SAS and SEA are combined to ASIA. Some sources having small
977 contributions are combined and shown as OTH.